Biomaterials Science

ROYAL SOCIETY OF CHEMISTRY

PAPER

View Article Online
View Journal | View Issue

Cite this: *Biomater. Sci.*, 2025, **13**, 6046

Modeling functional responses to pollutant exposure using modular hydrogel supported vascularized alveolosphere-on-a-chip

Sajeesh Kumar Madhurakkat Perikamana,†[a] Vardhman Kumar, †[b] Pankaj Mogha,[a] Lavonia Duncan,[b] Nikki Angel,[b] Aleksandra Tata,[c] Sairam V. Jabba,[d] Sven Eric Jordt,[d] Purushothama Rao Tata[c] and Shyni Varghese *[a,b,e]

Alveolar type 2 (AT2) cells play a pivotal role in maintaining lung homeostasis, and the generation of three-dimensional cultures, such as alveolospheres, provides a valuable model for studying lung development, pathologies, and drug responses. Here, we investigate the critical extracellular matrix (ECM) characteristics that influence AT2 alveolosphere formation and growth. By encapsulating AT2 cells in different extracellular matrix-based hydrogels, we identified laminin as a key ECM protein supporting robust alveolosphere formation akin to Matrigel. Our results show that laminin-rich hydrogels support alveolosphere formation across murine and human primary AT2 cells as well as induced human pluripotent stem cell derived AT2 cells (iAT2 cells). Notably, matrix stiffness strongly influenced alveolosphere formation. Hydrogels with a low Young's modulus and high compliance supported a greater number of alveolospheres, exhibiting a broader size distribution and a higher proportion of larger alveolospheres. Moreover, inhibition of matrix degradation and cellular contractility disrupted alveolosphere formation. Leveraging these insights, we developed a multicellular vascularized alveolosphere-on-a-chip model by integrating alveolospheres with endothelial cells and lung fibroblasts within a microfluidic device. Application of this model to assess the inflammatory effects of menthol, a common e-cigarette flavor, demonstrates its utility in evaluating the pulmonary effects of chemical exposures on alveolar cells. Our findings highlight the critical role of matrix physicochemical properties on alveolosphere formation and establish a versatile platform for advancing the study of lung biology, disease mechanisms, and drug discovery.

Received 11th April 2025,
Accepted 6th September 2025

DOI: 10.1039/d5bm00552c

rsc.li/biomaterials-science

Introduction

Alveoli, the tiny air sac like structures in the lung, are mainly responsible for gas exchange.[1] The alveolar epithelium is constantly exposed to the external environment and thus to various pathogens and air born particles.[2] Alveolar epithelial type 2 (AT2) cells serve as the predominant stem cell population in the lung alveoli.[3,4] Following alveolar injury, AT2 cells proliferate and differentiate to type 1 cells (AT1) to restore alveolar homeostasis.[4,5] AT2 cells produce surfactants that reduce the surface tension in the alveoli during gas exchange and also play a key role in the innate pulmonary immune defense.[6,7] Moreover, altered AT2 functions have been implicated in many lung pathologic conditions.[8–10]

While early *in vitro* studies utilized immortalized human cell lines to model lung diseases and homeostasis, the recent emergence of alveolus organoids, commonly termed as alveolospheres, has significantly advanced the application of cellular models for studying mechanisms driving alveolar stem cell self-renewal and differentiation in normal and pathological conditions. Given the key role played by the alveolar epithelial cells in lung tissue homeostasis and function, alveolospheres have been explored to model various lung diseases including those associated with SARS-CoV-2 infections.[11–13] Such models are expected to accelerate the discovery of new therapeutics; however, most of these 3D cell culture models utilize Matrigel, a cocktail of multiple ECM molecules and growth factors, to support the growth of the encapsulated cells and formation of alveolospheres. Due to the variability of ECM composition during Matrigel production, these models have been unreli-

[a]*Department of Orthopaedic Surgery, Duke University School of Medicine, Durham, NC, USA*
[b]*Department of Biomedical Engineering, Duke University, Durham, NC, USA. E-mail: shyni.varghese@duke.edu*
[c]*Department of Cell Biology, Duke University School of Medicine, Durham, NC, USA*
[d]*Department of Anesthesiology, Duke University School of Medicine, Durham, NC, USA*
[e]*Department of Mechanical Engineering and Materials Science, Duke University, Durham, NC, USA*
†These authors contributed equally to the manuscript.

able. The application of biomaterials with defined and tunable biophysical and biochemical properties enables the control over cellular biological responses, thereby expanding their utility.

One of the first studies to grow alveolospheres *in vitro* utilized a feeder cell population and serum containing medium.[4] Under these conditions, AT2 cells were shown to exhibit self-renewal and differentiation potential (into AT1 cells) when cultured in the presence of PDGFRα^{+} lung fibroblasts. A later study by Katsura *et al.* reported a defined, serum-free, and feeder-free culture condition that support alveolosphere formation when encapsulated in Matrigel.[11] Leveraging this defined medium, we examined the minimal, key extracellular matrix (ECM) protein(s) that are sufficient to support alveolosphere formation from progenitor or stem cells by employing primary AT2 cells and iPSC derived AT2 cells (Fig. 1A). Our studies identified laminin-111 as a key ECM protein that supported the formation of alveolospheres and long-term culture of AT2s. Three dimensional networks (*i.e.*, hydrogels) containing laminin enabled the growth and alveolosphere formation of encapsulated AT2 cells irrespective of the cell source (mice, human, and human iPSC derivatives). Employing this hydrogel system, we examined the role of matrix stiffness on AT2 cell growth and alveolosphere formation. Furthermore, we integrated the iAT2 organoids with a perfusable microvascular network and examined the potential of this platform to study environmental insults on alveolar epithelial cells and their effects on immune cell response. Together, the study described here provides a defined culture platform for AT2 alveolosphere formation and culture that can be vascularized

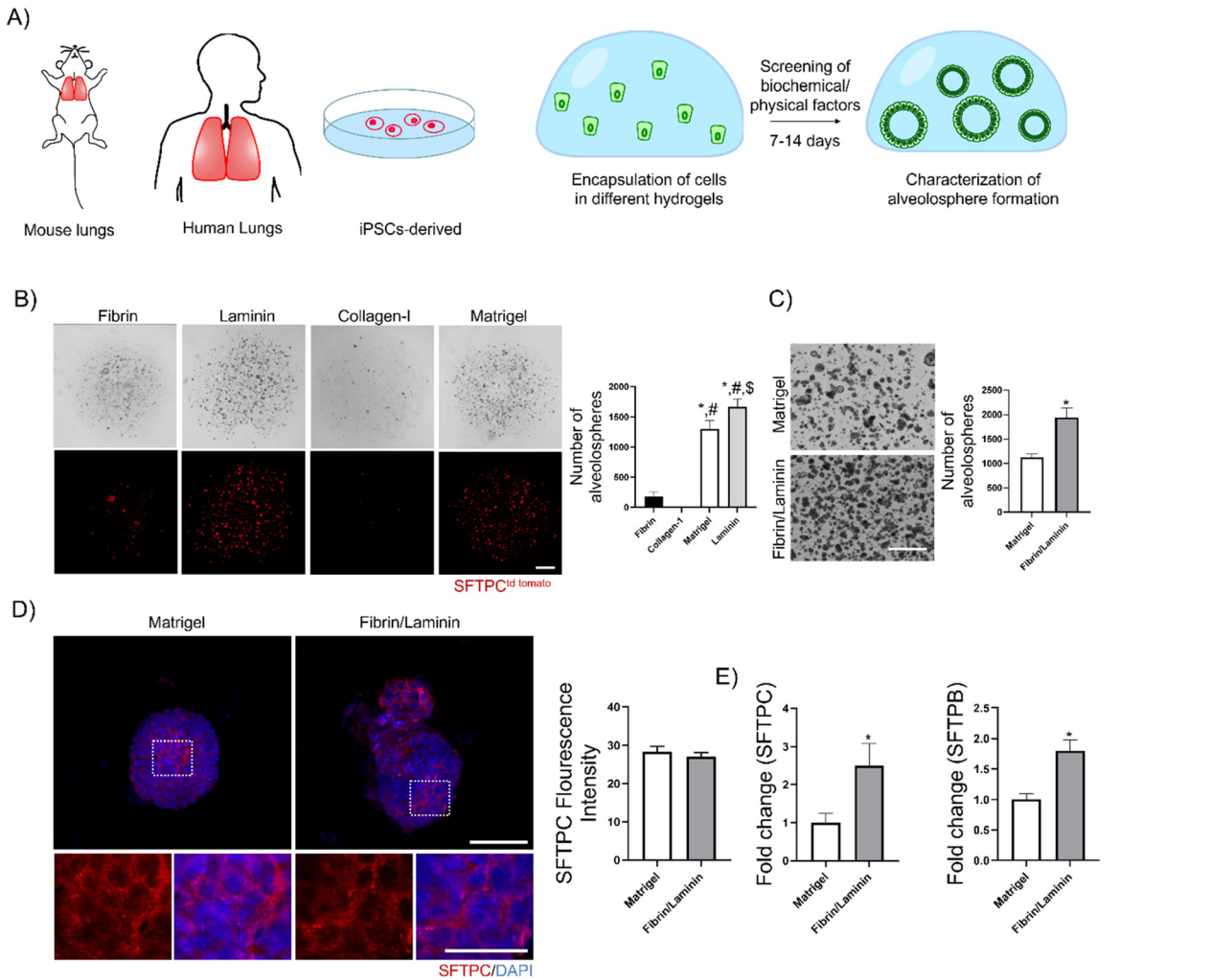

Fig. 1 Laminin-rich hydrogel supports alveolosphere formation: (A) AT2 cells from mouse, human, and hiPSC-derived were encapsulated into different ECM-based hydrogels, and alveolosphere formation was characterized. (B) Representative images and quantification iAT2-derived alveolospheres in different ECM-based hydrogels (n = 2–3). Scale bar: 2 mm. ("*", "#", and "$" indicate significant difference with fibrin, collagen type 1, and Matrigel respectively). (C) Representative images and quantification of iAT2-derived alveolospheres in Matrigel and fibrin/laminin hydrogel, respectively (n = 3). Scale bar: 500 μm. (D) Representative immunofluorescence staining images and quantification of SFTPC in iAT2-derived alveolospheres cultured in Matrigel and fibrin/laminin hydrogel, respectively (n = 3). Scale bar: 100 μm. (E) Gene expression analysis of AT2 cell markers SFTPC and SFTPB in iAT2-derived alveolospheres grown in Matrigel and fibrin/laminin hydrogel (n = 3).

and used to build complex and physiologically relevant models of the lung to study pulmonary physiopathology.

Results

Laminin rich hydrogels support AT2 alveolosphere formation

To identify the key ECM components that support the three-dimensional culture of alveolar epithelial stem cells, iPSC-derived AT2 (iAT2) cells were encapsulated in a three-dimensional hydrogel network made from either laminin 111, collagen type 1, or fibrin. These were compared against a Matrigel culture, the current gold standard. Experimental details of the hydrogel formation and AT2 encapsulations are provided in Materials and Methods. Analyses of the alveolosphere formation showed an ECM protein dependent effect with laminin hydrogels supporting AT2 organoid formation to a similar or greater extent than Matrigel (Fig. 1B). Specifically, organoid formation efficiency of AT2 cells seven days post encapsulation revealed higher alveolosphere formation in laminin hydrogels (1662.66 ± 128.81) compared to collagen type1 (2.5 ± 3.53) or fibrin (177.5 ± 82.73) hydrogels. The organoid formation efficiency was also found to be higher in laminin hydrogels than in Matrigel, with a value of 1306 ± 135.39. When extended to primary lung cells, specifically murine AT2 cells, laminin also supported their growth more effectively than collagen or fibrin hydrogels, with efficiency comparable to Matrigel cultures (Fig. S1A). Together, these data suggest that laminin could be a key ECM protein in supporting the growth of AT2 cells.

After identifying the ability of laminin hydrogels to support AT2 cell growth, we next examined the effect of laminin concentration on AT2 alveolosphere formation. Towards this, we leveraged fibrin hydrogels, formed by mixing fibrinogen with thrombin, containing varying concentrations of laminin. The laminin concentration varied from 1–10 mg ml^{-1} while keeping the fibrinogen concentration at 1.5 mg ml^{-1}. These semi-interpenetrating hydrogel networks (semi-IPN) were used to determine the effect of laminin concentration on AT2 alveolosphere formation and compared against the laminin only hydrogel (5 mg ml^{-1}) or Matrigel. Note that for laminin-only hydrogels, a concentration of 5 mg ml^{-1} was the minimum required to ensure stable hydrogel formation throughout the duration of cell culture (≥10 days). The sparsely encapsulated murine AT2 cells formed alveolospheres in all hydrogels, albeit with laminin concentration dependent differences. While hydrogel networks containing laminin supported alveolosphere formation, fibrin alone showed minimal alveolosphere formation. Similar to low concentration laminin only hydrogels, fibrin networks with 1 mg ml^{-1} laminin also disintegrated within 2–3 days post-gelation. Fibrin hydrogels (semi-IPN) with a laminin concentration of 3 mg ml^{-1} supported alveolosphere formation similar to that of laminin only hydrogel or Matrigel (Fig. S1B). Interestingly, further increase in laminin concentration to 5 or 10 mg ml^{-1} showed a decrease in alveolosphere formation. To investigate whether this was due to changes in mechanical properties, we assessed the stiffness of fibrin hydrogels with different laminin concentrations. Young's modulus, determined by atomic force microscopy (AFM), showed that hydrogels with 3 mg ml^{-1} laminin had a modulus of 25.46 ± 6.12 Pa, while those with 10 mg ml^{-1} had a modulus of 1660.22 ± 299.59 Pa.

Fibrin/laminin semi-IPN hydrogels with 3 mg ml^{-1} laminin also supported alveolosphere formation from human primary AT2 cells and iAT2 cells. Akin to the murine primary AT2 cells, the semi-IPN hydrogels containing 3 mg ml^{-1} laminin supported alveolosphere formation from human primary AT2 cells, similar to Matrigel (Fig. S1C). In the case of iAT2 cells, the alveolosphere formation was significantly higher in fibrin/laminin hydrogel than that in Matrigel (Fig. 1C). Immunostaining analysis of iAT2 alveolospheres for the AT2 marker surfactant protein C (SFTPC) suggests that these alveolospheres are enriched with AT2 cells (Fig. 1D), with no observed difference between fibrin/laminin and Matrigel cultures. Additionally, gene expression analysis of iAT2 cells showed higher expression of AT2 markers, SFTPC and surfactant protein B (SFTPB) in fibrin/laminin cultures compared to Matrigel cultures (Fig. 1E).

To further confirm the key role played by laminin in supporting AT2 alveolosphere formation, we replaced the fibrin network with either gelatin methacrylate (GelMA) or poly(ethylene glycol) diacrylate (PEGDA). Specifically, 3 mg ml^{-1} of laminin was incorporated into hydrogels formed from GelMA or PEGDA, and their ability to support alveolosphere formation from AT2 cells was examined. Although at a lower level compared to the fibrin/laminin network, GelMA and PEGDA networks containing laminin also supported the growth of the encapsulated murine AT2 cells and alveolosphere formation (Fig. S1D). The GelMA and PEGDA hydrogels by themselves showed no alveolosphere formation even after 10 days of culture. Among the GelMA and PEGDA hydrogels containing laminin, the GelMA/laminin hydrogel showed visibly more alveolospheres.

Matrix stiffness regulates alveolosphere formation

Having identified the laminin concentration that supports AT2 organoid formation, we next examined the effect of matrix stiffness on alveolosphere formation. To accomplish this, we varied the fibrinogen concentration (1.5–20 mg ml^{-1}) while keeping the laminin concentration constant at 3 mg ml^{-1} (Fig. 2A). A fibrinogen concentration of 1.5 mg ml^{-1} was found to be the lowest concentration that resulted in a stable hydrogel whose structural integrity was maintained over the course of the cell culture (≥10 days). Atomic force microscope (AFM) measurements were used to determine changes in Young's modulus of the fibrin/laminin semi-IPN hydrogels, which showed a fibrinogen-dependent increase in matrix stiffness (Fig. 2B and Table S1). Both iAT2 and murine primary AT2 cells displayed a matrix stiffness dependent change in alveolosphere formation (Fig. 2C and Fig. S2B). As revealed by the results in Fig. 2D, hydrogels with lower stiffness (*i.e.*, ~25 to ~250 Pa) supported similar alveolosphere formation from the

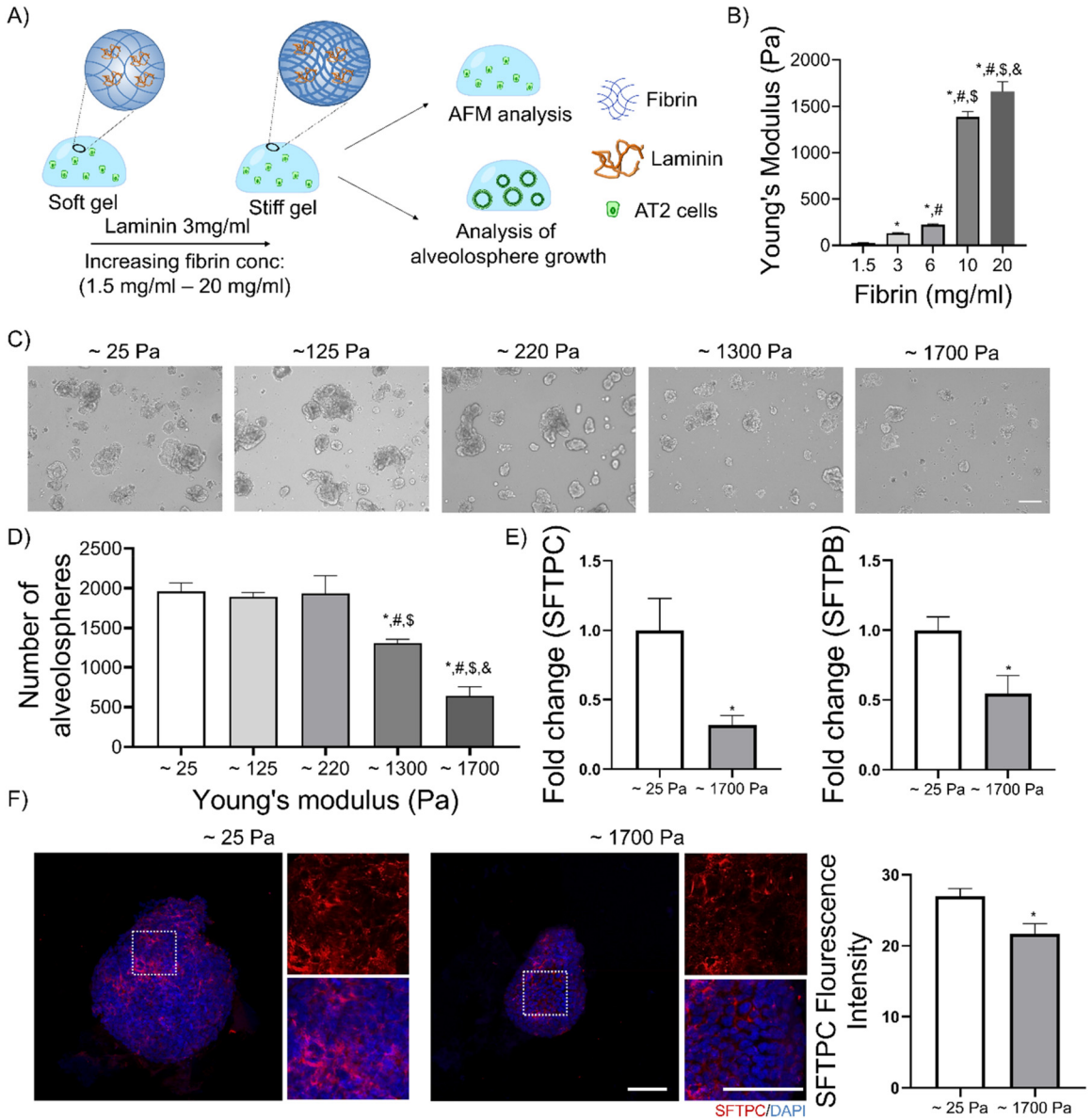

Fig. 2 Physicochemical properties of hydrogels influence the alveolosphere formation: (A) schematic showing the experimental procedures adapted for analyzing the effect of hydrogel stiffness on AT2 alveolosphere formation. (B) Storage modulus of fibrin hydrogels with different fibrinogen concentrations while keeping the laminin concentration constant ("*", "#", "$", and "&" indicate significant difference with 1.5, 3, 6, and 10 mg ml^{-1} fibrin, respectively). (C) Representative images of iAT2-derived alveolospheres within fibrin/laminin hydrogels with different stiffnesses. Scale bar: 150 μm. (D) Quantification of the number of iAT2-derived alveolospheres within the hydrogel with different stiffnesses (n = 4) ("*", "#", "$", and "&" indicate significant difference with ~25, ~125, ~230, and ~1300 Pa fibrin hydrogel, respectively). (E) Gene expression analysis of AT2 cell markers SFTPC and SFTPB in iAT2-derived alveolospheres grown in ~25 Pa and ~1200 Pa fibrin/laminin hydrogels (n = 3). (F) Representative immunofluorescence staining images and quantification of SFTPC in iAT2-derived alveolospheres cultured in ~25 Pa and ~1700 Pa fibrin/laminin hydrogel, respectively (n = 3). Scale bar: 100 μm.

encapsulated iAT2 cells, with these low-stiffness hydrogels fostering the highest number of alveolospheres. Increasing the matrix stiffness (>1000 Pa) led to a decline in the number of alveolospheres. The size of alveolospheres was also dependent on the hydrogel stiffness, with softer hydrogels supporting the formation of alveolospheres exhibiting a wide size distribution, including those exceeding 100 μm. In contrast, the stiffer hydrogel of ~1700 Pa mainly consisted of smaller alveolospheres (≤100 μm) (Fig. S2A). Calcein staining on day 14 showed comparable live cell staining among alveolospheres formed in Matrigel and in fibrin/laminin hydrogels with low and high stiffnesses (Fig. S2B). Consistent with this, gene expression analysis of the apoptotic marker Caspase-3 revealed no significant differences between alveolospheres cultured in fibrin/laminin hydrogels with low or high stiffness, with levels comparable to those in Matrigel (Fig. S2C). Alveolospheres in

high stiffness hydrogels (~1700 Pa) showed decreased expression of AT2 markers SFTPC and SFTPB compared to iAT2 cells in softer hydrogels (~25 Pa), as indicated by gene expression analysis (Fig. 2E). This trend was further supported by immunostaining, which revealed diminished SFTPC signal in alveolospheres formed within stiffer hydrogels compared to those in softer fibrin/laminin hydrogels. Cultures involving murine AT2 cells exhibited a similar trend: softer hydrogels facilitated the formation of a larger number of alveolospheres, whereas stiffer hydrogels resulted in significantly fewer alveolospheres (Fig. S2D).

Arresting contractility and material degradation inhibits alveolosphere formation

Given the importance of matrix degradation on organoid growth, we next examined the role of cell mediated matrix degradation on iAT2 alveolosphere formation by using a broad-spectrum protease inhibitor, GM600.[14] As anticipated, those cultured in the presence of GM6001 showed a significantly lower number of alveolosphere formation (Fig. S2E). Moreover, the alveolospheres in cultures containing GM6001 appeared visibly smaller in size. To determine the effect of cellular contractility on AT2 alveolosphere formation, we treated the cell-laden hydrogels with blebbistatin, a pharmacological inhibitor of myosin II.[15] Our results show that inhibiting cellular contractility with blebbistatin attenuated both the efficiency of alveolosphere formation and their growth (Fig. S2F and S2G).

Reconstituting multicellular vascularized alveoli-on-a-chip

We further utilized the ability of fibrin/laminin hydrogel to support alveolosphere formation to assemble a more complex multi-cellular model of the alveolus by incorporating other cell types (Fig. 3A). Specifically, we integrated the organoid with microfluidic-assisted microvascular network to create an alveoli-on-chip. Pre-generated alveolospheres (7 days in culture) were harvested and co-cultured with normal human lung fibroblasts (NHLFs) and human umbilical vein endothelial cells (HUVECs) within a multi-channel microfluidic device (Fig. 3B). The device consisted of three microchannels where the central channel was separated from the side channels *via* an array of trapezoidal micro posts.[16,17] The iAT2 alveolospheres of ~100 μm along with NHLFs and HUVECs were embedded in fibrin/laminin solution and injected into the central channel of the device. After hydrogel formation, medium was flushed into the side channels, and the cell-laden devices were cultured for an additional 5 days. During this time course, the endothelial cells self-organized into a microvascular network of capillary structures surrounding the alveolospheres (Fig. 3C). The multicellular vascularized alveoli-on-a-

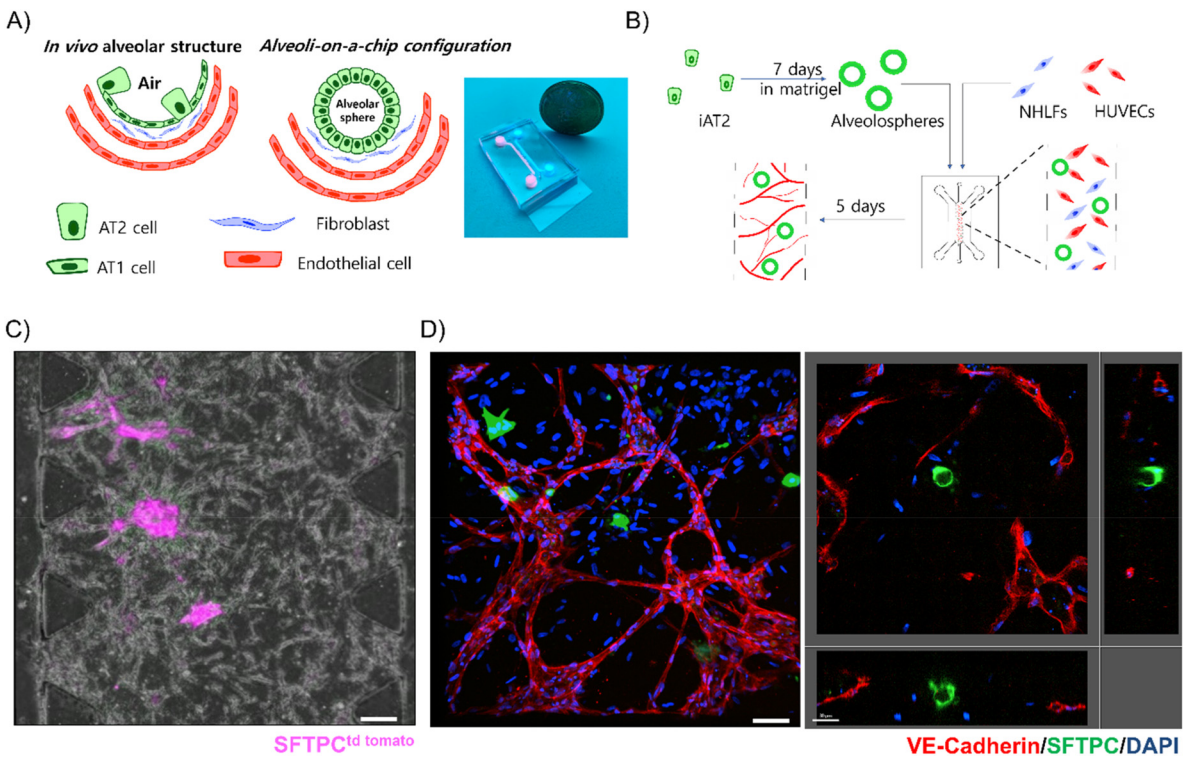

Fig. 3 Development of vascularized alveoli-on-a-chip: (A) schematic depiction of the lung alveoli and the assembly of multi-cellular alveoli-on-chip platform. A photograph of the alveoli-on-chip device is also provided. (B) Schematic showing the process of generating the vascularized alveoli-on-chip by co-culturing iAT2 alveolospheres, normal human lung fibroblasts (NHLFs), and human umbilical vein endothelial cells (HUVECs) within a microfluidic device. (C) Phase contrast image of the iAT2-incorporated vascularized alveoli-on-a-chip after 5 days of culture. (D) Characterization of the alveoli-on-a-chip using immunostaining for endothelial (VE-cadherin) and iAT2 (SFTPC) markers. Scale bar: 200 μm.

chip was characterized by immunostaining for pro-SFTPC (iAT2 cells), VE-cadherin (HUVECs), and vimentin (NHLFs) (Fig. 3D and S3A). These stains showed the presence of a vascular network with alveolospheres preserving their organoid structure and the phenotype.

Application of vascularized alveoli-on-a-chip to evaluate the effect of a pulmonary irritant

We utilized the vascularized alveoli-on-a-chip to determine its potential to assess the effect of chemical exposure on lung cells, by using menthol, a popular flavor component of e-cigarette liquids, as a model molecule. Specifically, we examined the effect of menthol on inducing inflammation and subsequent immune cell recruitment (Fig. 4A). TNFα, a known pro-inflammatory molecule which is linked to a number of pulmonary diseases, was used as a positive control.[18,19] Treatment with menthol and TNFα led to a significant increase in VCAM-1, an indicator of inflamed endothelium, in the vascular network (Fig. 4B and C). We next perfused fluorescently labeled human neutrophils into the vasculature and quantified their adhesion within the network. Akin to TNFα treatment, menthol treatment was found to result in a significant increase in adhesion and accumulation of neutrophils (Fig. 4D and E). Although not statistically significant, similar to TNFα treatment, alveolospheres exposed to menthol showed a reduction in SFTPC expression (Fig. 4F and G). These findings are consistent with the established inflammatory effect of menthol.[20,21] Our studies further suggest that vascularized alveoli-on-chip that can emulate the respiratory effects of pulmonary irritants and chemical exposure and could be a physiologically relevant platform towards screening of various molecules.

Discussion

Organoids have emerged as a valuable tool for modeling organogenesis, pathophysiology, and for use as a platform for drug screening.[22] The advent of organoids has enabled the long term culture of primary lung epithelial cells, an achievement that remained elusive for years. With optimized medium conditions, organoids from various regions of the lung—trachea, airway, and alveoli—have been cultured by embedding them in a 3D basement membrane matrix, Matrigel.[23] Alveolospheres, organoids derived from AT2 cells are increasingly being used to study lung morphogenesis, functions, and pathologies, including SARS-CoV-2 infections.[24]

Advances are being made to control the organoid assembly by employing defined matrices, incorporating microfluidics, and bioprinting.[25–27] While alternatives to Matrigel and matrix-free cultures have been explored to reduce variabilities in the 3D self-assembly of the cells, further advances are needed to understand the role of cell–matrix interactions on organoid formation and tailor the matrices to engineer multicellular tissues with complex and *in vivo* like structure and function.[28] Recent studies by Loebel *et al.* show that synthetic hyaluronic acid (HA) hydrogel-based microwells support the alveolosphere formation of AT2 cells.[29] By examining the effect of several key ECM molecules, we identified laminin-111 as a critical ECM protein that supports the maintenance of AT2 cells and the formation of alveolospheres, similar to Matrigel. The presence of laminin supported alveolosphere formation when used alone or in combination with other materials that support cell attachment such as fibrin or gelatinLaminin-rich hydrogels have been shown to support various organoids such as intestinal and liver.[30,31]

Incorporation of laminin within fibrin hydrogels, semi-IPN, enabled independent control over mechanical properties of the hydrogel by varying the fibrinogen concentration while keeping the laminin content constant. Assembly of alveolospheres in fibrin/laminin hydrogels required cell-mediated degradation of the hydrogel as demonstrated by inhibition of proteases which significantly reduced organoid formation. Pharmacological inhibition of contractility was also found to reduce organoid formation, thus suggesting the importance of cytoskeletal mechanics in organoid formation within the fibrin–laminin hydrogels. These findings are consistent with other studies including ours that showed the importance of both degradation and matrix compliance on the growth of organoids or spheroids within a 3D matrix.[14,25]

We next harnessed the ability of fibrin/laminin supported AT2 cultures to create a multicellular alveoli-on-chip by integrating the alveolospheres within a microfluidic device and co-culturing with endothelial cells and primary lung fibroblasts. Previously, we showed that endothelial cells in fibrin hydrogels self-organized into lumenized microvascular networks.[16,17]

We utilized the multicellular alveoli-on-a-chip to model inflammation associated with flavors present in e-cigarette liquids. A steep increase in e-cigarette use has led to the incorporation of novel flavors to increase their marketability and appeal. Menthol is one of the most common flavors used because of its mint flavor and cooling effects.[32] A number of studies have reported the harmful effect of menthol on lung cells both *in vitro* and *in vivo*.[20,33] Perfusion of menthol into the vascular network and its exposure to the alveolospheres resulted in an increase in VCAM-1 expression in the endothelium, accompanied by enhanced neutrophil recruitment. We also observed a slight decline in SFTPC expression after menthol exposure. These findings are in agreement with reported effects of menthol on lung cells as demonstrated by 2D cells cultures and in mice models where menthol has been shown to have an inflammatory effect on endothelial cells.[34,35] Recent studies have also indicated that e-cigarette flavors, especially menthol, can induce epithelial-to-mesenchymal transition of alveolar epithelial cells and inhibit the production of pulmonary surfactants.[36,37]

While the multicellular alveoli-on-a-chip platform offers an advanced cellular model by incorporating human cells in 3D architectures that mimic the epithelial, interstitial, and endothelial compartments of the alveoli, it does not fully recapitulate all features of native lung tissue. For instance, the current platform is static and lacks the dynamic mechanical functions

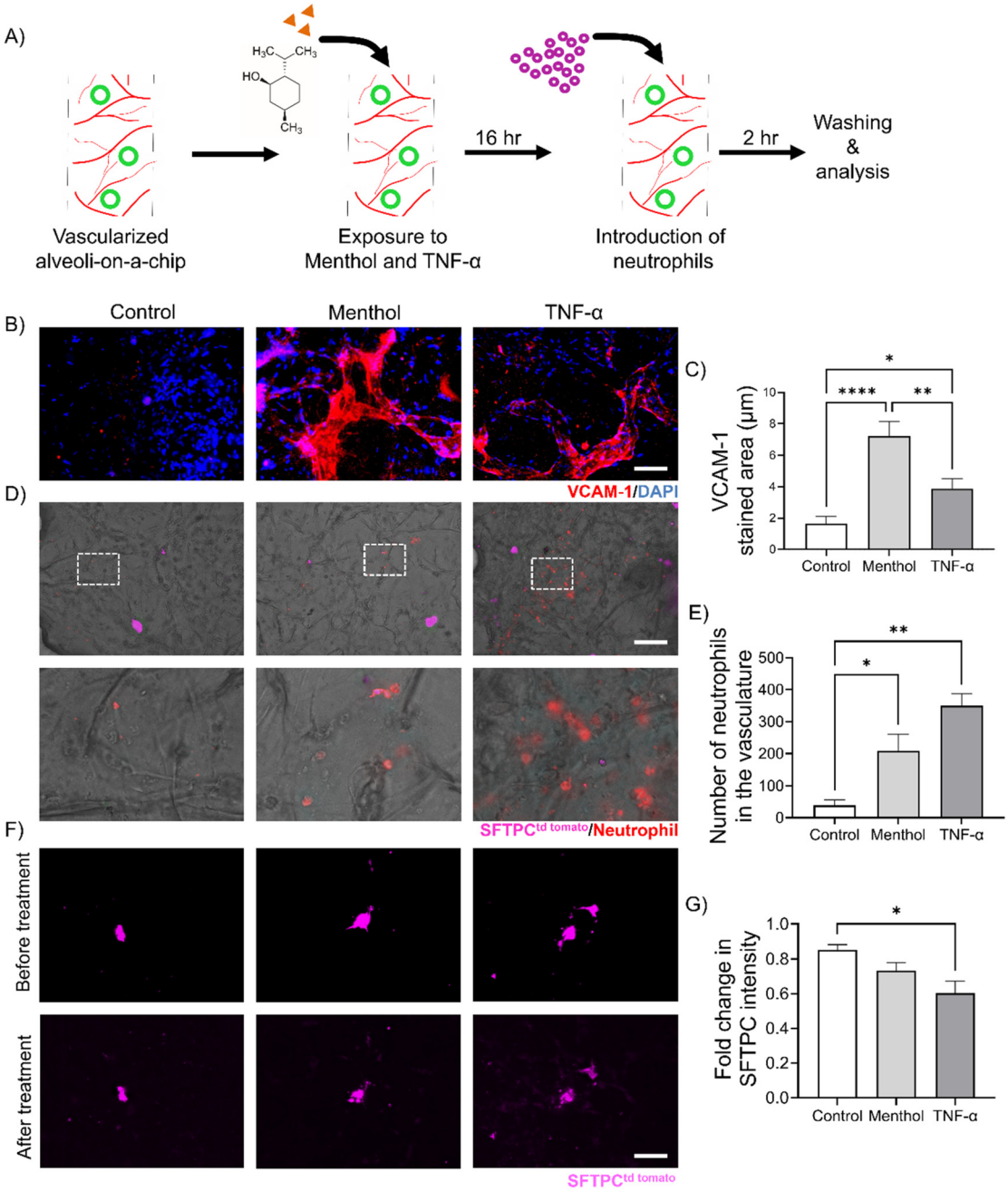

Fig. 4 Pulmonary pollutants induce inflammatory response in the vascularized alveoli-on-a-chip: (A) schematic representation of the experimental procedure used to assess the inflammatory response of the multi-cellular alveoli following the exposure to menthol using the vascularized alveoli-on-a-chip. (B) Representative images and (C) quantification of VCAM-1 expression following exposure to menthol or TNF-α (n = 3). Scale bar: 100 μm. (D) Representative images and (E) Quantification of fluorescently labeled human neutrophils adhesion to the vascularized alveoli after exposure to menthol or TNF-α (n = 3). Scale bar: 500 μm. (F) Representative images of SFTPC-positive alveolospheres in the vascularized alveoli-on-a-chip following exposure to menthol or TNF-α. (G) Quantification of SFTPC intensity of the alveolospheres after exposure to menthol and TNF-α within the vascularized alveoli-on-a-chip (n = 3). Scale bar: 200 μm.

associated with breathing. Nevertheless, the microfluidic system can be further engineered to incorporate breathing-associated mechanical cues, as we have previously described.[33] Another limitation of our model is that it includes only alveolar type 2 (AT2) cells and therefore does not fully represent the epithelial cellular composition of the alveoli. Further studies are needed to identify culture conditions that support the differentiation of precursor cells into alveolar type 1 (AT1) cells[40,41] and their co-maintenance with AT2 cells within the device. Despite these limitations, the model remains a valuable tool for investigating lung-specific disease processes and the role of AT2 cells in pathogenesis.

Conclusion

In summary, this study provides a bottom-up design to engineer complex multicellular models of tissues by tailoring ECM properties and cell–ECM interactions. We identified and tuned the key physio-chemical properties of an ECM-based hydrogel to culture alveolospheres in a defined matrix. We found that soft laminin or laminin-rich hydrogels were able to support alveolosphere formation. Cell-mediated hydrogel degradation and cellular contractility were also found to be essential for alveolosphere growth in this system. We utilized this hydrogel platform to create a multicellular alveoli-on-a-chip by integration into a microfluidic device and co-culture of alveolospheres with fibroblasts and self-assembled vasculature. The alveoli-on-a-chip was utilized to study the effect of a highly popular and marketed e-cigarette flavor, menthol, on inflammation and neutrophil trafficking within the alveoli. The framework developed here can be further developed to incorporate other lung regions (airway, trachea) and can also be applied to build models of organs beyond the lung.

Experimental section

Isolation of mouse AT2 cells

All animal procedures were performed in accordance with the Guidelines for Care and Use of Laboratory Animals of Duke university and approved by the Animal Ethics Committee of Duke university. Lung dissociation was performed as described previously.[11,38] Briefly, lungs were inflated with a dissociation enzyme solution containing 450 U mL^{-1} *Collagenase I* (Worthington, LS004197), 5 U mL^{-1} *Dispase* (Corning, 354235), and 0.33 U mL^{-1} *DNase I* (Roche, 10104159001). Lung lobes were separated, minced and incubated in an enzyme solution at 37 °C for 25–35 min. Dissociation was quenched with DMEM/F12 + 10% FBS medium and strained through a 100 μm cell strainer. The cell pellet was resuspended in red blood cell lysis buffer for 2 min, followed by quenching with DMEM/F12 + 10% FBS and filtration through a 40 μm strainer. For FACS sorting, the cell pellet was resuspended in a DMEM/F12 + 2% FBS medium. Sorting was performed using either a SONY SH800S or SONY MA900. FACS-sorted AT2 cells were resuspended in serum-free, feeder-free (SFFF) media and mixed with Matrigel in droplet format. After Matrigel solidification at 37 °C for 20–30 min, the mouse SFFF medium was added.

Isolation of human AT2 cells

Excised sub-transplant-quality human lung tissues from donors without preexisting chronic lung diseases were obtained from the BioRepository & Precision Pathology Center (BRPC), Duke university. Human AT2 cells were isolated as described previously.[11,38] Briefly, following pleura removal, airway and vasculature were micro dissected, and the remaining human lung tissue (approximately 3 g) was minced and digested with an enzyme mixture (450 U mL^{-1} *Collagenase type I*; 5 U ml^{-1} *Dispase*; 10 U ml^{-1} *DNaseI*) at 37 °C for 1 h with rotation. Dissociation was quenched with DMEM/F12 + 10% FBS and filtered through a 100 μm cell strainer and centrifuged at 450*g* for 5 min. Pellet was resuspended in red blood cell lysis buffer, incubated for 5 min at room temperature and quenched with DMEM/F12 + 10% FBS. Sample was filtered through a 40 μm cell strainer and cells were centrifuged at 450*g* for 5 min at 4 °C and the cell pellet was processed for AT2 isolation. Briefly, about 2–10 million total lung cells were suspended in MACS buffer and incubated with Human TruStain FcX (BioLegend, #422032) for 15 min at 4 °C followed by incubation with HTII-280 antibody for 1 h at 4 °C. The cells were washed and incubated with anti-mouse IgM microbeads for 20–30 min at 4 °C. The cells were loaded into the LS column (Miltenyi Biotec, # 130-042-401) and labelled cells were collected magnetically.

iAT2 culture

Human iPSC derived alveolar cells were obtained from the Kotton Lab at Boston u = University.[39] Single cells of iAT2s were encapsulated in 60% v/v Matrigel (Corning, 354230) and cultured in Iscove's modified Dulbecco's medium (IMDM)/Ham's F12 media containing 3 μg CHIR99021, 10 ng mL^{-1} KGF, 50×10^{-6} M dexamethasone, 0.1×10^{-3} M 3-isobutyl-1-methylxanthine (IBMX), 43 μg mL^{-1} 8-bromo-cAMP, and primocin; this medium is called CK + DCI medium. Cells were supplemented with 1 μM of Y-27632 (Stemcell Tech, 72302) for the first 48 hours of culture and then replenished with CK + DCI media without Y-27632, and the media was replaced with an equal amount of medium every 3–4 days. The resulting iAT2 spheres were passaged every 12–17 days. For passaging, the cell-laden Matrigel cultures were initially digested with 2 mg ml^{-1} dispase (MilliporeSigma, D4693-1G) for 30 min at 37 °C, followed by incubation with 0.05% trypsin (ThermoFisher Scientific, 25300062) for 5 min to obtain a single cell suspension. The single cells were encapsulated within the Matrigel (60% v/v) as described above and cultured to expand the cells.

Identifying ECM that supports AT2 cell growth

Mouse AT2 cells, human AT2 cells, or iAT2s were released from Matrigel cultures, by enzymatic digestion using trypsin, to form a single cell suspension. To identify the ECM proteins that support growth of AT2 cells, we conducted an initial screening using 3D cultures of AT2 cells in collagen type 1 (Corning, 354236), laminin-111 (Corning, 354259) or fibrinogen (Alfa Aesar, J63276), encapsulating 2000 cells per hydrogel for mouse and human AT2 cells and 8000 cells per hydrogel for iAT2 cells.

For encapsulation of AT2 cells in a collagen gel, the single cells were resuspended in 3 mg ml^{-1} collagen containing 0.1 M sodium hydroxide (NaOH) in sterile PBS. Collagen solution dispersed with the cells were placed as a 20 μl cell suspension onto a tissue culture plate. The culture was left for 30 min at 37 °C to ensure complete gelation of collagen, following which the culture medium was added.

For cell encapsulation in laminin hydrogels, the single cells were resuspended in 5 mg ml^{-1} laminin solution in cell culture medium and 20 μl of the cell suspension was placed on a well plate and allowed for gelation for 20 min at 37 °C. Cell encapsulation into fibrin hydrogel was performed by resuspending the single cells in 3 mg ml^{-1} fibrinogen solution in saline and to which 0.5 U ml^{-1} of thrombin (Sigma, T6634-500UN) was added to induce gelation. 20 μl of the cell suspension was immediately placed onto a well plate and allowed for gelation for 30 min at 37 °C. The cell-laden hydrogels were cultured in CK + DCI medium with 10 μM Y-27632 for the first 48 h and thereafter in CK + DCI medium without Y-27632.

Fabrication of fibrin hydrogels with various laminin concentrations

To optimize the laminin concentration needed for supporting the AT2 cell growth, different concentrations of laminin (3–5 mg ml^{-1}) were mixed with the fibrin solution (1.5 mg ml^{-1}) containing mouse AT2 cells and supplemented with 0.5 U ml^{-1} of thrombin to induce the gelation and immediately placed onto a well plate. After the gelation, culture media was added onto the well plate and cultures were maintained for 10 days. Media was changed every 3–4 days.

Cell encapsulation into GelMA and PEGDA hydrogels

Gelatin methacrylate (GelMA) and polyethylene glycol diacrylate (PEGDA) were synthesized as previously described.[40,41] For the encapsulation of AT2 cells into GelMA hydrogel, GelMA was initially dissolved in PBS to create a 10% w/v solution. Further, 10% w/v GelMA solution was supplemented with the photoinitiator LAP (2 mM) and mixed with the AT2 cells. The same combination was also supplemented with 3 mg ml^{-1} laminin to prepare a GelMA/laminin hydrogel solution. 20 μl of the cells containing GelMA or GelMA/laminin solution were then pipetted onto a well plate and photopolymerized for 30 seconds. After gelation, culture medium was added to the well plate, and cultures were maintained for 10 days. Medium was changed every 3–4 days. For the cell encapsulation into PEGDA hydrogel, a 10% PEGDA (w/v in PBS) was prepared and mixed with the photoinitiator LAP (2 mM), 10 μg ml^{-1} poly-D-lysine (Sigma, P7886), and AT2 cells. The mixture with and without the laminin was pipetted onto a well plate and photopolymerized for 30 seconds. Cells containing PEGDA hydrogels were cultured in mouse AT2 media and maintained for 10 days with regular media changes.

Fabrication of fibrin/laminin hydrogels of various stiffness

Fibrin/laminin hydrogels with various stiffnesses were prepared by increasing the fibrinogen concentration while keeping the laminin concentration constant. Cells were initially mixed with various concentrations of fibrinogen (1.5–20 mg ml^{-1}) and to this 3 mg ml^{-1} laminin were added. To this cell mixture, 0.5 U ml^{-1} of thrombin was added to induce gelation. After ensuring the complete gelation after 30 min, hydrogels containing cells were cultured with culture media as described earlier. Cultures were continued for 10 days for mouse AT2 cells and 14 days for iAT2 cells with regular media changes.

Hydrogel characterization by AFM

To determine the elastic modulus, hydrogel samples with varying fibrinogen or laminin concentrations were directly polymerized on microscope slides. The samples were submerged in PBS, and atomic force microscopy (AFM) measurements were done with a custom-made borosilicate glass particle (20 μm) attached to silicon nitride cantilever with a nominal spring constant of 0.1 N m^{-1} (Novascan on MFP-3D, Asylum Research) in contact mode. After contact was made, the force distance was set to 7 μm, the velocity to 700 μm s^{-1}, and the trigger point to 1 V. The AFM measurements were carried as described by us earlier.[42] At least 24 force curves were collected for each sample. The force curves were fitted to the Hertizian model, corrected for finite thickness, to determine the Young's modulus.

Effect of cell contractility and degradability

To determine the effect of cell contractility and hydrogel degradability on alveolosphere formation, the cultures were supplemented with blebbistatin (Millipore Sigma, 203389) or broad spectrum MMP inhibitor GM6001, respectively. Specifically, the cell-laden hydrogels were cultured in media containing 12.5 μM of blebbistatin or 10 μM of GM6001. Cultures were maintained for 10 days for mouse AT2 cells and 14 days for iAT2 cells with regular media replenishments.

Calcein staining

Cell viability in alveolospheres was assessed by calcein staining. On day 14, iAT2 alveolospheres cultured in Matrigel, as well as in soft and stiff fibrin/laminin matrices, were incubated with calcein dye (2 μM; Thermo Fisher Scientific, Cat# C1430) in culture medium for 20 minutes. Following incubation, the samples were gently washed with PBS. Fluorescence imaging was performed using a Keyence BZ-X700 fluorescence microscope.

Immunostaining

Alveolosphere-laden hydrogels were fixed with 4% paraformaldehyde (PFA) in PBS for 30 min. Hydrogels were then disrupted by pipetting to extract the alveolospheres and centrifuged at 500 rpm for 1 min to collect the cells, which were then washed with distilled water. The organoids were then spread onto glass slides and allowed to attach by air drying. Subsequently, organoids were rehydrated with PBS and permeabilized with 0.2% Triton X-100 (Sigma-Aldrich, X100) in PBS for 15 min and blocked with 2.5% normal donkey serum in PBS for 1 h. Samples were then incubated with primary antibodies against SFTPC (Sigma, AB3786) at a 1 : 300 dilution in blocking buffer overnight at 4 °C. Subsequently, samples were washed with PBS and incubated with Alexa 647 donkey–rabbit (Jackson ImmunoResearch Laboratories, 711-605-152) at a 1 : 250 dilution in blocking buffer along with Hoechst 33342 (2 μg mL^{-1}; Thermo Fisher) for 1 h at room temperature.

Samples were washed, mounted using mounting media, and imaged using a Keyence BZ-X700 microscope or Dragonfly confocal microscope.

RNA isolation and qRT PCR

RNA was extracted with TRIzol, phase-separated with chloroform, precipitated with isopropanol, and washed with 70% ethanol. One microgram of RNA was reverse transcribed with iScript cDNA Synthesis Kit (Bio-Rad, Hercules, CA, Cat# 1708891) according to the manufacturer's instructions. Quantitative PCR was conducted using the iTaq Universal SYBR green reagent (Bio-Rad, Cat# 1725124) on a QuantStudio 3 PCR cycler (ThermoFisher). The thermal cycling conditions included an initial denaturation at 95 °C for 30 s for one cycle, and amplification (denaturation + annealing/extension) at 95 °C for 5 s and 60 °C for 30 s for 40 cycles.

The primer sequences used are: SFTPC (forward, CACCTGAAACGCCTTCTTATCG; reverse, TTTCTGGCTCATGTGGAGACC), SFTPB (forward, CTTCCAGAACCAGACTGACTCA; reverse, GCTCGGAGAGATCCTGTGTG), ACTB (forward, CGTCACCAACTGGGACGACA; reverse, CTTCTCGCGGTTGGCCTTGG), and CASPASE-3 (forward, TCTGGTTTTCGGTGGGTGTG; reverse, CGCTTCCATGTATGATCTTTGGTT). The expression level of each target gene was normalized to the housekeeping gene and to their respective controls and presented as fold change.

Image analysis

Phase contrast *Z*-stacks images were acquired through the entire regions of the alveolosphere hydrogels. Alveolosphere numbers and diameters were quantified using FIJI ImageJ software. Alveolospheres were defined as three-dimensional spheroids measuring at least 30 μm in diameter with well-defined boundaries; smaller clusters or loosely connected cells were excluded. Fluorescence intensity was quantified using ImageJ from single-channel images corresponding to the marker of interest. Regions of interest (ROIs) were manually selected using the freehand selection tools to outline the alveolosphere areas and the mean grey value was measured. Measurements were performed across multiple organoids and in three experimental replicates.

Fabrication of the microfluidic device

The photomask for photolithography was designed in AutoCAD and printed at a high resolution on a transparency film. 10 mm diameter silicon wafers were cleaned, mounted on a spin coater and approximately 4 ml of SU-8 100 (MicroChem) was poured on the wafer. The SU-8 was spin coated at 3000 rpm for 30 seconds. The wafer was then baked at 65 °C for 10 min and 95 °C for 30 min before exposing it to UV light through the photomask. Post exposure, the wafer was baked at 65 °C for 1 min and at 95 °C for 10 min. The wafer was then immersed in SU-8 developer for 15 min to remove unexposed/uncured SU-8 before cleaning with isopropanol and drying at 60 °C overnight. The next day, the wafer was treated with trichloro(1*H*,1*H*,2*H*,2*H*-perfluorooctyl) silane (Sigma, 448931) by using vapor deposition in a desiccator for 15 min. After this process, the wafer was kept on a hot plate at 100 °C for 30 min to remove excess silane. The wafer was attached to the bottom of a 15 cm-diameter Petri dish. PDMS (base: cross-linker: 9 : 1) was poured onto the wafer and the Petri dish was kept in a desiccator for 1 h. After degasification, the wafer with PDMS was placed in an oven at 60 °C for 2 h to allow the PDMS to cure. After curing, PDMS was cut around the features and inlets and outlets were created by punching holes at the ends of the three microchannels. A 1 mm diameter biopsy punch was used to create the inlet and outlet for the central hydrogel microchannel, and a 4 mm diameter biopsy punch was used to create inlets and outlets for medium microchannels. After punching the inlets and outlets, scotch tape was put on all sides on the PDMS to prevent dust adhesion. Rectangular cover glasses (50 mm × 24 mm) were cleaned using 1 N NaOH for 15 min on an orbital shaker followed by washing with distilled water and drying them. Scotch tape was removed from the PDMS substrates. The PDMS and cleaned cover glass were treated with oxygen plasma to activate the surfaces for bonding. Post oxygen plasma/corona treatment, the PDMS and glass were bonded by bringing them in contact and gently pressing them to remove air from between the surfaces. The bonded devices were then placed in an oven for at least 1 h to strengthen the glass-PDMS bonding.

Vascularized alveolospheres

HUVECs and NHLFs were purchased from Lonza (CC-2519 and CC-2512, respectively). Human umbilical vein endothelial cells (HUVECs) were maintained in EGM-2MV media (CC-3202), and normal human lung fibroblasts (NHLFs) were maintained in FGM-2 fibroblast growth media from Lonza (CC3132). Cells were trypsinized upon reaching 80% confluency. HUVECs, NHLFs, and alveolospheres were harvested and combined at a ratio of 7 : 1 : 0.1, respectively. The cell mixture was centrifuged and resuspended in 3.96 U ml^{-1} thrombin diluted in EGM-2MV. After pelleting the cells again, they were resuspended in 3.96 U ml^{-1} thrombin: EGM-2MV to achieve a concentration of 50 M ml^{-1} with respect to HUVECs. This cell suspension was then mixed with a 1 : 1 (equal volumes) mixture of fibrinogen : laminin, and the resulting solution was pipetted into the gel loading inlet of the devices. Subsequently, the loaded devices were placed in a humidification chamber at room temperature for 15 min. After incubation, EGM-2MV was flushed into the devices through the media channels to ensure complete filling of the reservoirs (inlet ports of media). Media change was performed daily for the devices.

Effect of menthol on vascularized alveoli-on-a-chip

Potential respiratory and vascular effects of pulmonary chemical exposures were analyzed on the vascularized alveoli-on-a-chip using L(−)-menthol (125401000, Thermo Fisher Scientific) or TNF-α (R&D systems, 210-TA-005), which was used as the positive control. 1 mM of menthol or 100 ng ml^{-1} TNF-α was introduced into the media channel of the vascularized alveoli-on-chip platform and cultured for 16 h. Subsequently, media

containing menthol or TNF-α was removed and washed with PBS three times. Human neutrophils (# IQB-Hu1-Nu10, IQ Bioscience) labeled with Cell Tracker Red CMTPX (Invitrogen), at a density of 1×10^4 cells, were then introduced through the channel and cultured for another 2 h. The device was then washed with PBS three times and subsequent analyses were performed.

Immunostaining of vascularized alveoli-on-a-chip

Cells within the chip were fixed by perfusing 4% PFA in the media microchannels for 30 min followed by permeabilizing with 0.2% Triton X-100 in PBS for 30 min. Subsequently, cells were blocked with 2.5% normal donkey serum for 2 h. Primary antibodies corresponding to SFTPC (1 : 300), VE-cadherin (1 : 200, R&D systems, AF938-SP), Vimentin (1 : 500, Millipore sigma, V6630), or VCAM-1 (1 : 50, Thermo Fisher, MA5-11447) were diluted in blocking buffer and incubated at 4 °C overnight. The device was then washed thrice with PBS and incubated with donkey anti-rabbit Alexa Fluor 647 (1 : 300) or donkey anti-Mouse Alexa Fluor 647 (1 : 500, Thermo Fisher, A-31571) secondary antibodies and Hoechst for nuclei (1 : 2000) for 2 h. Samples were washed with PBS and imaged using a Keyence BZ-X710 fluorescence Microscope or Andor Dragonfly Spinning Disk Confocal Plus microscope.

Statistical analysis

An unpaired two tailed Student's *t*-test in GraphPad Prism 10.2.1 was utilized for comparing two groups, while for multiple group comparisons, statistical significance was determined using one-way analysis of variance (ANOVA) with *post hoc* Tukey's test, also conducted in GraphPad Prism 10.2.1. Results were considered statistically significant if the *p*-value was less than 0.05, and all data were presented as a means with standard deviations.

Conflicts of interest

The authors declare no conflict of interest.

Data availability

All data supporting the findings of this study are available within the article and its SI files. Supplementary information is available. See DOI: **https://doi.org/10.1039/d5bm00552c**.

Raw data are available from the corresponding author upon reasonable request.

Acknowledgements

The study is partially supported Kaganv Research Initiative Grant from Duke, NCATS/NIH (3UH3TR002142–04S1), and NCI/NIH (R01CA251407). P. R. T would like to acknowledge support from NHLBI/NIH (R01HL160939 and R01HL153375). S. V. J. and S. E. J. acknowledge support from NIDA/NIH (R01DA060884), the Center for Tobacco Products of the U.S. Food and Drug Administration (FDA), and the NIEHS/NIH Chemical Countermeasures Program (CCRP) (R01ES034387).

The authors also acknowledge Duke Cancer Institute Flow Cytometry Shared Resource (DCI-FCSR) for cells sorter and Duke University Shared Materials Instrumentation Facility (SMIF), a member of the North Carolina Research Triangle Nanotechnology Network (RTNN), which is supported by the National Science Foundation (award number ECCS-2025064) as part of the National Nanotechnology Coordinated Infrastructure (NNCI).

The sponsors had no role in the design and conduct of the study; collection, management, analysis, and interpretation of the data; preparation, review, or approval of the manuscript; and decision to submit the manuscript for publication. The content is solely the responsibility of the authors and does not necessarily represent the views of the funding agencies.

References

1 J. C. Schittny, *Cell Tissue Res.*, 2017, **367**, 427–444.
2 J. A. Whitsett and T. E. Weaver, *Am. J. Respir. Cell Mol. Biol.*, 2015, **53**, 1–7.
3 B. L. Hogan, C. E. Barkauskas, H. A. Chapman, J. A. Epstein, R. Jain, C. C. Hsia, L. Niklason, E. Calle, A. Le and S. H. Randell, *Cell Stem Cell*, 2014, **15**, 123–138.
4 C. E. Barkauskas, M. J. Cronce, C. R. Rackley, E. J. Bowie, D. R. Keene, B. R. Stripp, S. H. Randell, P. W. Noble and B. L. Hogan, *J. Clin. Invest.*, 2013, **123**, 3025–3036.
5 P. R. Tata and J. Rajagopal, *Development*, 2017, **144**, 755–766.
6 E. Crouch and J. R. Wright, *Annu. Rev. Physiol.*, 2001, **63**, 521.
7 A. M. Olajuyin, X. Zhang and H.-L. Ji, *Cell Death Discovery*, 2019, **5**, 1–11.
8 A. Mulay, B. Konda, G. Garcia Jr, C. Yao, S. Beil, J. M. Villalba, C. Koziol, C. Sen, A. Purkayastha and J. K. Kolls, *Cell Rep.*, 2021, **35**, 109055.
9 T. H. Sisson, M. Mendez, K. Choi, N. Subbotina, A. Courey, A. Cunningham, A. Dave, J. F. Engelhardt, X. Liu and E. S. White, *Am. J. Respir. Crit. Care Med.*, 2010, **181**, 254–263.
10 C. Yao, X. Guan, G. Carraro, T. Parimon, X. Liu, G. Huang, A. Mulay, H. J. Soukiasian, G. David and S. S. Weigt, *Am. J. Respir. Crit. Care Med.*, 2021, **203**, 707–717.
11 H. Katsura, V. Sontake, A. Tata, Y. Kobayashi, C. E. Edwards, B. E. Heaton, A. Konkimalla, T. Asakura, Y. Mikami and E. J. Fritch, *Cell Stem Cell*, 2020, **27**, 890–904.
12 Y. Korogi, S. Gotoh, S. Ikeo, Y. Yamamoto, N. Sone, K. Tamai, S. Konishi, T. Nagasaki, H. Matsumoto and I. Ito, *Stem Cell Rep.*, 2019, **12**, 431–440.
13 T. Suezawa, S. Kanagaki, K. Moriguchi, A. Masui, K. Nakao, M. Toyomoto, K. Tamai, R. Mikawa, T. Hirai and K. Murakami, *Stem Cell Rep.*, 2021, **16**, 2973–2987.

14 A. Aung, S. K. Davey, J. Theprungsirikul, V. Kumar and S. Varghese, *Adv. Healthcare Mater.*, 2023, **12**, 2201842.
15 M. Kovács, J. Tóth, C. Hetényi, A. Málnási-Csizmadia and J. R. Sellers, *J. Biol. Chem.*, 2004, **279**, 35557–35563.
16 N. R. Natesh, P. Mogha, A. Chen, S. J. Antonia and S. Varghese, *APL Bioeng.*, 2024, **8**, 016120.
17 V. Kumar, D. Kingsley, S. M. Perikamana, P. Mogha, C. R. Goodwin and S. Varghese, *Biofabrication*, 2023, **15**, 035008.
18 R. Malaviya, J. D. Laskin and D. L. Laskin, *Pharmacol. Ther.*, 2017, **180**, 90–98.
19 L. K. Lundblad, J. Thompson-Figueroa, T. Leclair, M. J. Sullivan, M. E. Poynter, C. G. Irvin and J. H. Bates, *Am. J. Respir. Crit. Care Med.*, 2005, **171**, 1363–1370.
20 J. Herbert, J. S. Kelty, J. D. Laskin, D. L. Laskin and A. J. Gow, *Am. J. Physiol.: Lung Cell. Mol. Physiol.*, 2023, **324**, L345–L357.
21 T. Muthumalage and I. Rahman, *Toxicol. Sci.*, 2023, **193**, 146–165.
22 G. Rossi, A. Manfrin and M. P. Lutolf, *Nat. Rev. Genet.*, 2018, **19**, 671–687.
23 J. Kong, S. Wen, W. Cao, P. Yue, X. Xu, Y. Zhang, L. Luo, T. Chen, L. Li and F. Wang, *Stem Cell Res. Ther.*, 2021, **12**, 1–13.
24 J. Wang, X. Li, A. Wang, F. Zhao, Q. Wu, L. Li, H. Yu, J. Wu and H. Chen, *Cell Proliferation*, 2020, **53**, e12928.
25 N. Gjorevski, N. Sachs, A. Manfrin, S. Giger, M. E. Bragina, P. Ordóñez-Morán, H. Clevers and M. P. Lutolf, *Nature*, 2016, **539**, 560–564.
26 G. Saorin, I. Caligiuri and F. Rizzolio, *Semin. Cell Dev. Biol.*, 2023, **144**, 41–54.
27 J. A. Brassard, M. Nikolaev, T. Hübscher, M. Hofer and M. P. Lutolf, *Nat. Mater.*, 2021, **20**, 22–29.
28 S. A. Yi, Y. Zhang, C. Rathnam, T. Pongkulapa and K. B. Lee, *Adv. Mater.*, 2021, **33**, 2007949.
29 C. Loebel, A. I. Weiner, M. K. Eiken, J. B. Katzen, M. P. Morley, V. Bala, F. L. Cardenas-Diaz, M. D. Davidson, K. Shiraishi and M. C. Basil, *Adv. Mater.*, 2022, **34**, 2202992.
30 N. Broguiere, L. Isenmann, C. Hirt, T. Ringel, S. Placzek, E. Cavalli, F. Ringnalda, L. Villiger, R. Züllig and R. Lehmann, *Adv. Mater.*, 2018, **30**, 1801621.
31 G. Sorrentino, S. Rezakhani, E. Yildiz, S. Nuciforo, M. H. Heim, M. P. Lutolf and K. Schoonjans, *Nat. Commun.*, 2020, **11**, 3416.
32 M. C. Diaz, E. M. Donovan, B. A. Schillo and D. Vallone, *Tobacco Control*, 2021, **30**, 700–703.
33 Z. Liu, C. Li, L. Mu, H. Hu and X. Qin, *Clin. Respir. J.*, 2023, **17**, 1265–1275.
34 S. Majid, R. M. Weisbrod, J. L. Fetterman, R. J. Keith, S. H. Rizvi, Y. Zhou, L. Behrooz, R. M. Robertson, A. Bhatnagar and D. J. Conklin, *PLoS One*, 2023, **18**, e0280674.
35 M. J. Mears, H. L. Hookfin, P. Bandaru, P. Vidal, K. I. Stanford and L. E. Wold, *Circ. Res.*, 2023, **132**, 1168–1180.
36 A. Zahedi, R. Phandthong, A. Chaili, G. Remark and P. Talbot, *Lung Cancer*, 2018, **122**, 224–233.
37 Q. Wang, J. H. Lucas, C. Pang, R. Zhao and I. Rahman, *Respir. Res.*, 2024, **25**, 23.
38 S. Konishi, A. Tata and P. R. Tata, *STAR Protoc.*, 2022, **3**, 101447.
39 A. Jacob, M. Morley, F. Hawkins, K. B. McCauley, J. Jean, H. Heins, C.-L. Na, T. E. Weaver, M. Vedaie and K. Hurley, *Cell Stem Cell*, 2017, **21**, 472–488.
40 N. Seale, S. Ramaswamy, Y.-R. Shih, I. Verma and S. Varghese, *Transplantation*, 2018, **102**, e373–e381.
41 S. K. Davey, A. Aung, G. Agrawal, H. L. Lim, M. Kar and S. Varghese, *Tissue Eng., Part C*, 2015, **21**, 1188–1196.
42 A. Aung, Y. N. Seo, S. Lu, Y. Wang, C. Jamora, J. C. del Álamo and S. Varghese, *Biophys. J.*, 2014, **107**, 2528–2537.